



COLLÈGE  
DE FRANCE  
1530



Internship report

Collège de France - Kastler Brossel Laboratory

---

# Improving the atom transport in an ultracold Dysprosium atoms setup

---

*Author :*  
Mr. Louis FOLLET

*Supervisor :*  
Prof. Sylvain NASCIMBÈNE

école \_\_\_\_\_  
normale \_\_\_\_\_  
supérieure \_\_\_\_\_  
paris – saclay \_\_\_\_\_

Version of  
September 1, 2023

Submitted in Partial Fulfillment of the Requirements for the Degrees of:

- *Diplôme de l'Ecole Normale Supérieure Paris-Saclay*, Physics department, Ecole Normale Supérieure Paris-Saclay
- *Diplôme d'ingénieur*, Institut d'Optique Graduate School
- Master of Science in Physics, Quantum-Light-Matter-Nanoscience track, Paris-Saclay University

# Acknowledgements

First of all, I would like to thank Sylvain for the opportunity he gave me to join the Dysprosium team. His approach to problems is very inspiring and I can only take it as an example for my future career.

Then, a big thank you to the team, Jean-Baptiste, Quentin, Nehal, Aurélien and Chi, who helped me understand a very complex setup and guided me throughout my project.

I also really enjoyed spending time together outside the lab, so thank you for making these few months of internship super enjoyable!

# Abstract

In cold atoms experiments, the number of atoms reaching the science cell is a limiting factor in the type of experiment that can be performed. The main goal of this internship is thus a technical upgrade of the current setup.

We first demonstrate through numerical simulations that an improvement in atom transport is possible, by modulating the beam to create a time-averaged potential which optimizes the atomic cloud trapping.

To this end, we design and build a new setup comprising an acousto-optic modulator and a high-power laser. This new apparatus is finally tested to demonstrate its performance.

# Table of Contents

<b>Acknowledgements</b>	<b>2</b>
<b>Abstract</b>	<b>3</b>
<b>1 Introduction</b>	<b>5</b>
<b>2 Motivations</b>	<b>7</b>
2.1 Overview of the experimental setup . . . . .	7
2.2 Optical dipole trap and transport optical setup . . . . .	10
2.2.1 Principle of Optical Dipole Traps . . . . .	10
2.2.2 Current transport ODT setup . . . . .	12
2.3 Science cell and evaporative cooling . . . . .	14
2.3.1 Science cell . . . . .	14
2.3.2 Basics of evaporative cooling . . . . .	15
2.4 Outlook . . . . .	16
<b>3 Improving the transport laser</b>	<b>18</b>
3.1 Theory and simulations . . . . .	18
3.1.1 Principle of time-averaged potentials . . . . .	18
3.1.2 Choice of the modulation function . . . . .	20
3.1.3 Tuning the aspect ratio . . . . .	23
3.2 Experimental setup . . . . .	25
3.2.1 New transport setup . . . . .	25
3.2.2 Imaging the beam . . . . .	27
3.2.3 Working with high power . . . . .	29
3.2.4 The acousto-optic modulator . . . . .	31
3.3 Modulation results . . . . .	34
3.3.1 Atom trapping configuration . . . . .	34
3.3.2 Beam modulation . . . . .	34
<b>Conclusion</b>	<b>39</b>

# Chapter 1

## Introduction

In 1981, Richard Feynman declared during one of his lectures "Nature isn't classical, dammit, and if you want to make a simulation of nature, you'd better make it quantum mechanical", followed by an article that launched the era of quantum simulation [1]. Since then, numerous simulation platforms have emerged, ranging from superconducting quantum circuits to trapped ions and ultracold atoms. Each one of these platforms has its own specificities, enabling the simulation of diverse systems and phenomena such as quantum materials or nonequilibrium quantum many-body dynamics. It is in the context of the latter type of problem that the physics of ultracold atoms has emerged as a reference for quantum simulation. Two main approaches can be distinguished. The first one consists in highly coherent quantum systems with hundreds of individually addressed quantum elements, so-called Rydberg atom arrays. Using optical tweezers, this type of bottom-up approach can for instance enable the simulation of the antiferromagnetic two-dimensional transverse-field Ising model [2], a typical many-body problem. The second approach uses ultracold neutral atoms working with thousands to tens of millions of interacting fermionic or bosonic quantum elements, with high degree of isolation, flexible geometry, interaction and spin control, and slow observable dynamics. These properties enable the study of a broad range of paradigmatic quantum phases and phenomena [3] [4].

This field of research is at the heart of the "Quantum gases" group of the Kastler Brossel Laboratory at Collège de France, supervised by Prof. Jean Dalibard. During my internship, I joined the "Dysprosium" team led by Prof. Sylvain Nascimbène, which is interested in the study of various states of quantum matter using ultracold dysprosium atoms. One specificity of this atomic element is its large angular momentum  $J=8$ , enabling a strong coupling between the spin of atoms and their motion (see fig 1.1a). This makes it possible to create artificial magnetic fields [5], and to observe, for example, the physics of the quantum Hall effect (see fig 1.1b), with a spatial dimension and a second encoded in the discrete magnetic sublevels [6].

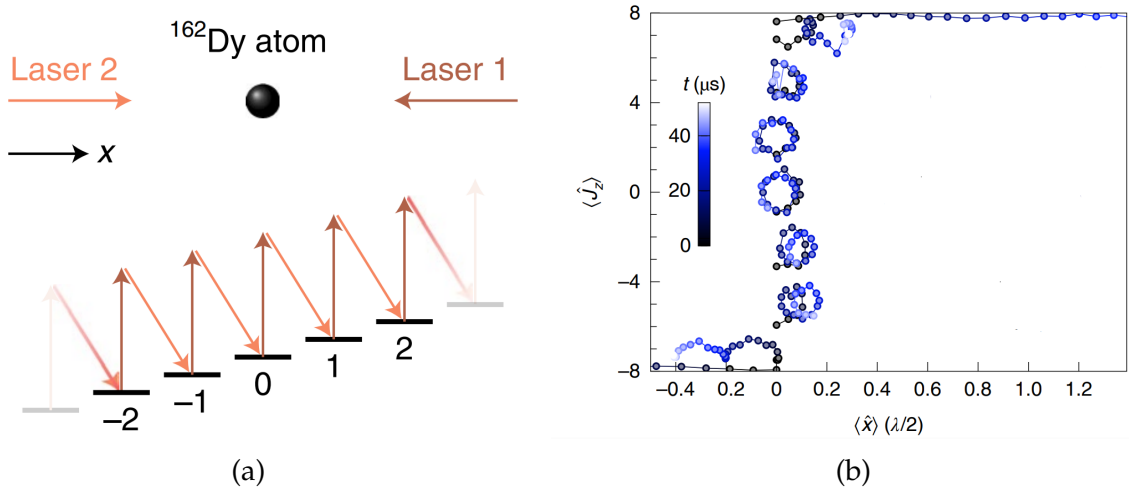


Figure 1.1: **Figures adapted from [6].** (a) The atom dynamics are induced by two-photon optical transitions coupling successive magnetic sublevels  $m$ . (b) Trajectories in  $(x, m)$  space showing cyclotron and skipping orbits typical of a quantum Hall system and its Landau level structure.

The ongoing project during my internship dealt with the experimental realization of the entanglement Hamiltonian of a topological quantum Hall system [7], but due to the advanced stage of the project and the short duration of my stay, we decided that my work would focus mainly on an experimental upgrade of the setup, on the transport laser, which I present in this report. In the next chapters, I will justify the need for such an upgrade, before presenting the theory and the experimental setup behind our improvements, and finally our results.

# Chapter 2

## Motivations

In this chapter, I will describe the main experimental setup, in order to motivate my work on the setup upgrade. As a typical quantum gases experiment, our main goal is to bring a hot vapor of dysprosium to an ultracold sample of dysprosium atoms. Depending on the aimed project, the number of atoms remaining at the end of the process can be important, especially for experiments requiring a Bose-Einstein Condensate (BEC). We will see that on the current machine, upgrading the transport of the thermal cloud could greatly improve this number of atoms.

### 2.1 Overview of the experimental setup

As every cold atom experimental setup, our machine is quite complex and contains many different parts, all of them being essential to our experiments. To keep the description brief, I will here only give an overview of the most important ones. More detailed discussions on the experimental apparatus can be found in [8][9].

The whole setup is a combination of a high vacuum system and a laser system, and a simplified scheme is given in 2.1. The vacuum part, represented by the different ion pumps on the scheme, simply prevents the perturbations from other particles on our dysprosium atoms, improving their lifetimes. The laser systems is used for most steps of the experiments : the light-atoms interactions enable us to slow the atoms, trap them, cool them and engineer exotic Hamiltonians for quantum simulation purposes.

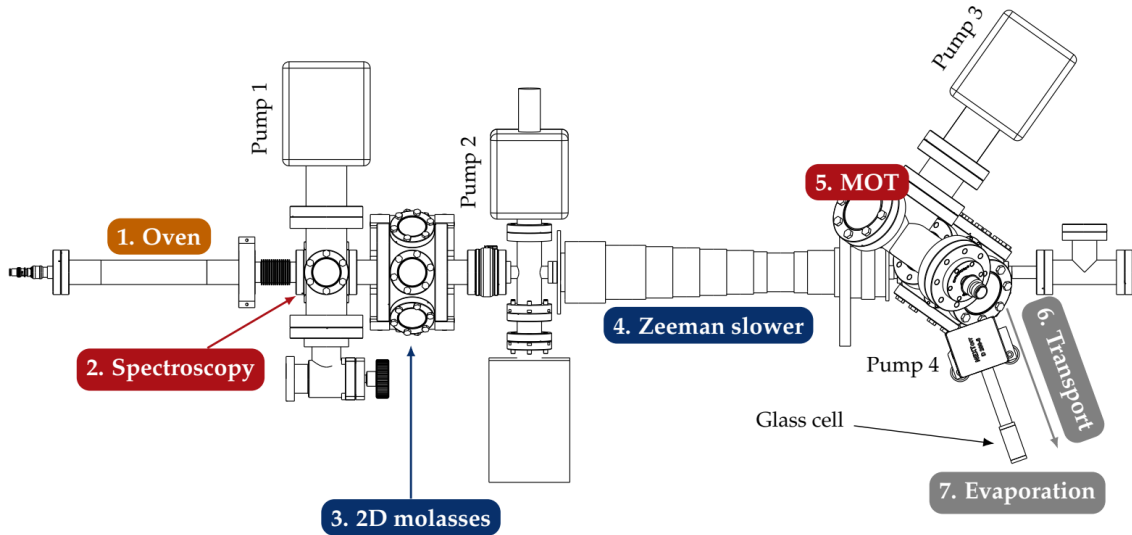


Figure 2.1: Global scheme of the experimental apparatus. [10]

We describe below the main parts of the apparatus :

### 1. Effusion oven

An evaporation oven heats up metallic dysprosium cut in millimetre-sized granules to about 1100 °C in order to reach its vapor pressure. The created vapor then exits the oven as a so-called “atomic beam” through a collimation tube, with a velocity of about 500 ms<sup>-1</sup>.

### 2. Spectroscopy

In the following parts, the two transitions that we use ( $\lambda = 421$  nm and  $\lambda = 626$  nm) either for cooling or imaging, are addressed using a blue and a red laser. It requires a precise frequency tuning close to the optical transition, and we use a feedback loop to actively tune the absolute frequency of our lasers, thanks to saturated absorption spectroscopy[11].

### 3. Transverse cooling

At the output of the oven, the atomic beam is still relatively diverging. We implement a transverse cooling scheme by using laser beams propagating in a direction orthogonal to the atomic jet. Their frequency is red-detuned from the 421 nm transition in the lab frame, so that they are Doppler shifted to the resonant frequency in the moving frame. By reducing the transverse velocity distribution, we increase the flux of atoms reaching the Zeeman slower.

#### 4. Zeeman slower

In order to reach the capture velocity of our magneto-optical trap of about  $8 \text{ ms}^{-1}$ , we use a counter-propagating 421 nm laser beam to reduce the longitudinal velocity of the atomic jet over 50 cm. While the atoms are cooled, the laser is no longer in resonance with their blue transition. To compensate this Doppler effect, we apply a spatially-varying magnetic field that shifts the resonance frequency of our atoms by Zeeman effect.

#### 5. Magneto-optical trap

The apparatus consists in two coils in an anti-Helmholtz configuration to create a magnetic field and three pairs of counter-propagating laser beams, of chosen intensities and detuning. These parameters enable us to control the temperature and the density of the atomic cloud. We use here the red laser to address the narrow 621 nm transition. The cooling is limited down to the Doppler limit[11]:  $T_{DL} = \hbar\Gamma_{red}/(2k_B) \approx 3.2 \text{ K}$ , typically lower than reachable temperatures using alkali atoms.

Since we are using dysprosium, a lanthanide specie with a large atomic mass, the non-negligable contribution of the gravitation competes with the trapping induced by the magnetic gradient and the light. The equilibrium position of our magneto-optical trap (MOT) is thus below the zero-crossing of the magnetic gradient, lifting the degeneracy of the ground state manifold. The MOT is then spin-polarised by the laser beams in the absolute ground state  $|J = 8, m_J = -8\rangle$ , enabling us to describe the MOT as a two-level system with an excited state  $|J' = 9, m'_J = -9\rangle$  [12]. Moreover, this spin-polarized regime enhances the Doppler cooling and the trapping of the atoms in the next experimental steps.

We typically trap about  $5 \times 10^7$  atoms at a temperature of  $T = 15 \mu\text{K}$ , above the Doppler temperature but sufficiently low to transport them.

#### 6. Transport

We load the compressed atomic cloud in a far-detuned optical dipole trap (ODT). On the current setup, we use a 50 W, multi-mode fiber-amplified laser<sup>1</sup> at 1070 nm for the ODT. We focus it on the MOT, and the atoms are transported to the science cell – the final part of our apparatus – over 28 cm by shifting the focal point of the ODT, using a translation stage that varies the length of the optical path. With the current configuration (see fig 2.2), the efficiency of the loading and transporting stages is about 1 – 10%, giving us about  $10^6$  atoms in the science cell at a temperature about  $100 \mu\text{K}$ . We will discuss in more detail the theory of ODT, the current transport setup and its limitation in the next part.

---

<sup>1</sup>YLR 50 W, IPG Photonics

## 7. Science cell and evaporation

Once the atomic cloud is transported to the science cell, we apply again Doppler cooling using a red-detuned beam, and we transfer the atoms from the transport beam to crossed optical dipole traps (cODT), consisting in two single-mode laser beams at 1064 nm that intersect at the focal point of the laser beam. Their waist is about 25  $\mu\text{m}$ , and we use a modulation technique to increase the effective beam width of one of them. The overlap between the transport beam and the cODT is suboptimal due to the loose longitudinal confinement in the transport Gaussian beam. We will entirely describe the modulation technique and how to improve this overlap in Chapter 3.

Finally, we decrease the intensity of the ODTs to force the evaporative cooling – that we will describe at the end of this chapter – down to Bose-Einstein condensation if the atomic cloud is dense enough.

## 2.2 Optical dipole trap and transport optical setup

### 2.2.1 Principle of Optical Dipole Traps

Optical trapping of atoms relies on the interaction between an atom and a light field far detuned from any optical transition. In this regime, the interaction potential induced by a laser beam on an atom is

$$U_{dip}(\mathbf{r}) = -\frac{I(\mathbf{r})}{2\epsilon_0 c} \text{Re}(\alpha) \quad (2.1)$$

where  $I(\mathbf{r})$  designates the light intensity that depends on position, and  $\text{Re}(\alpha)$  is the real part of the atomic polarizability.

Strickly speaking,  $\alpha$  depends on the internal state of the atom. Even though these spin-dependent terms are the building blocks of how we engineer and study light-spin interactions, we will here focus on the spin-independent part of the polarizability: the scalar part of  $\alpha$ . Since  $\text{Re}(\alpha)$  is positive[13], the overall coupling is therefore attractive.

We consider a cylindrical symmetry around the propagation axis  $z$ , so we can write  $\rho = \sqrt{x^2 + y^2}$ , where  $\rho$  indicates the distance from the axis. We can then write the intensity profile of a gaussian beam as

$$I(\mathbf{r}) = I(\rho, z) = I_0 \left( \frac{w_0}{w(z)} \right)^2 \exp \left( \frac{-2\rho^2}{w(z)^2} \right). \quad (2.2)$$

In this expression,  $z = 0$  is by convention the position of the focal point, where the beam has a minimal waist  $w_0$ . The beam then expands in the  $z$  direction following the formula

$$w(z) = w_0 \sqrt{1 + \left(\frac{z}{z_R}\right)^2} \quad (2.3)$$

where  $z_R = \pi w_0^2 / \lambda$  is the Rayleigh length. The maximum intensity  $I_0$  is directly related to the total laser power  $P$ , as

$$I_0 = \frac{2P}{\pi w_0^2}. \quad (2.4)$$

The corresponding dipole potential is then

$$U(\rho, z) = -U_0 \left( \frac{w_0}{w(z)} \right)^2 \exp \left( \frac{-2\rho^2}{w(z)^2} \right) \quad (2.5)$$

where the total trap depth  $U_0$  is given by

$$U_0 = -U_{dip}(\rho = 0, z = 0) = \frac{I_0}{2\epsilon_0 c} \text{Re}(\alpha). \quad (2.6)$$

By performing a Taylor expansion of the expression of  $U(\mathbf{r})$  to the second order around its maximum at  $\mathbf{r} = \mathbf{0}$ , one can extract the trap frequencies corresponding to the transverse and the longitudinal confinements. Indeed, we obtain the expression

$$U(\rho, z) \approx -U_0 \left[ 1 - 2 \left( \frac{\rho}{w_0} \right)^2 - \left( \frac{z}{z_R} \right)^2 \right]. \quad (2.7)$$

One can recognize a 3-dimensional harmonic potential as

$$U(\rho, z) \approx -U_0 + \frac{m}{2} \left[ \omega_\rho^2 \rho^2 + \omega_z^2 z^2 \right] \quad (2.8)$$

with  $\omega_\rho$  and  $\omega_z$  being respectively the transverse and axial trap frequencies

$$\omega_\rho = \sqrt{\frac{4U_0}{mw_0^2}} \quad \text{and} \quad \omega_z = \sqrt{\frac{2U_0}{mz_R^2}}. \quad (2.9)$$

We define the *aspect ratio* as  $\frac{\omega_\rho}{\omega_z}$ , so we have here

$$\frac{\omega_\rho}{\omega_z} = \frac{\sqrt{2}\pi w_0}{\lambda} \gg 1. \quad (2.10)$$

The confinement is much stronger in the transverse direction, leading to an elongated trap along the axial direction. By combining two orthogonal beams of the same wavelength, one can obtain a more spherical trap, which frequencies will be deduced by the transverse single-beam frequencies : this is the principle of the so-called crossed optical dipole traps (cODT) described earlier. As we will see in Chapter 3, we can modulate the laser beam to tune the ODT frequencies, which means tuning the atomic cloud shape, in order to improve the transport of our atoms.

### 2.2.2 Current transport ODT setup

The ODT described previously is the main tool we use to transport atoms. The current optical transport setup is given below in figure 2.2. The first part of the system is composed of half-wave plates and a polarizing cube, to filter the polarization and to control the power. The beam is then broadened using a telescope and focused on the atoms in the MOT by a +800 mm converging lens. Thanks to a moving stage, we can shorten the optical path before the MOT chamber and then move the focal point up the science cell.

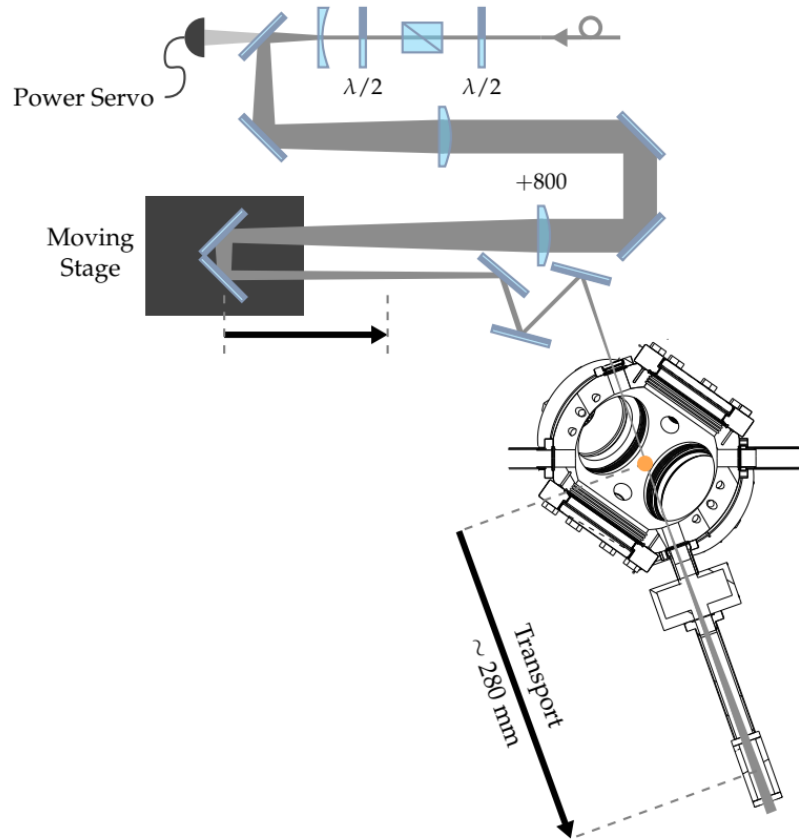


Figure 2.2: Current transport setup [10]

Currently, the transport system is not optimal and we lose a non-negligible number of atoms during this process. The main reasons are :

- The **volume of the optical dipole trap** is small compared to the size of MOT, leading to a loading efficiency of about 10%,
- The vacuum is not perfect, leading to a relatively low collisional lifetime of the atoms. However, to keep the transport in the adiabatic regime, the transport time still needs to be longer than the timescale associated to the **axial frequency of the trap**. This frequency is thus an important parameter to take into account.

## 2.3 Science cell and evaporative cooling

### 2.3.1 Science cell

The science cell - or glass cell - is the last step of the experiment, where we perform the final atoms cooling and realize the real physics experiments. We transfer the atoms to this separated cell in order to have better optical access to the atoms compared to the MOT. We give a scheme of the cell in fig 2.3:

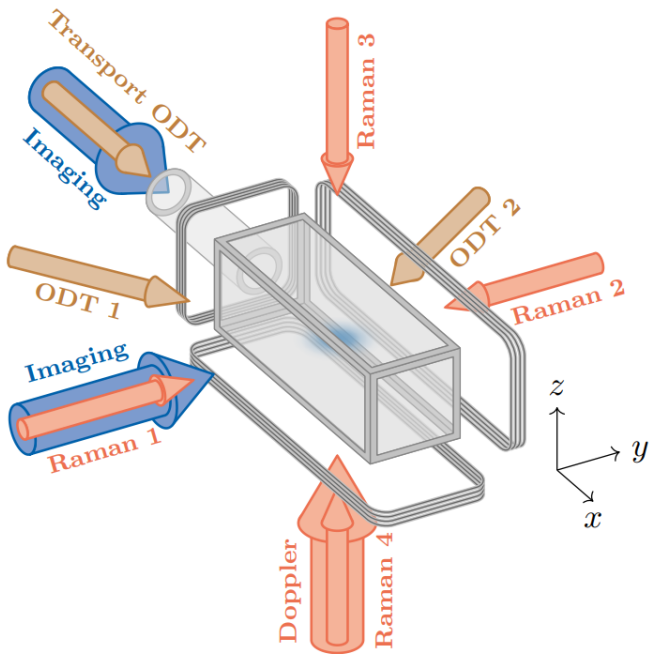


Figure 2.3: **Science cell scheme.** [11] The glass cell and the surrounding magnetic coils are depicted in grey. The dipole traps, the imaging beams, the Doppler beam the Raman beams are respectively shown as small brown, large blue, large red and small red arrows.

We can see on this figure the different beams sent to the atoms.

- As we described earlier, we apply Doppler cooling by using a Doppler beam and rectangular magnetic coils, shown in grey.
- The role of the so-called Raman beams is to address the atoms and to induce spin dynamics and spin-orbit coupling, to perform complex experiments, as discussed earlier in the introduction.

- The imaging beams are the main measurement tool, based on absorption imaging with a single-spin resolution. To give a simple description, it consists sending to the atomic a large resonant laser beam, leading to photon absorption. Since the photons are re-emitted in random direction by spontaneous emission, the atoms appear as a shadow on the image recorded on a CCD camera.
- As discussed briefly before, the atoms are transferred to the cODT using the transport beam.

The transport ODT is elongated in the axial direction and narrow in the transverse one, the overlap with the cODT is relatively poor, and leads to a **loss of atoms in the loading process**. Once the atoms loaded, we lower the ODTs intensities to force evaporation cooling, which will be briefly described in the next part.

### 2.3.2 Basics of evaporative cooling

This process can be summarized as follows[14]: we let the high-energy atoms in the cloud to escape the trap, leading to a decrease of the average energy per particle, and thus an overall cooling of the cloud. By lowering down the intensity of the cODT, we lower the trap depth and set free the hottest atoms, while the remaining ones thermalize thanks to elastic collision, leading to a lower temperature of the atomic gas. A scheme of this process is given in fig 2.4:

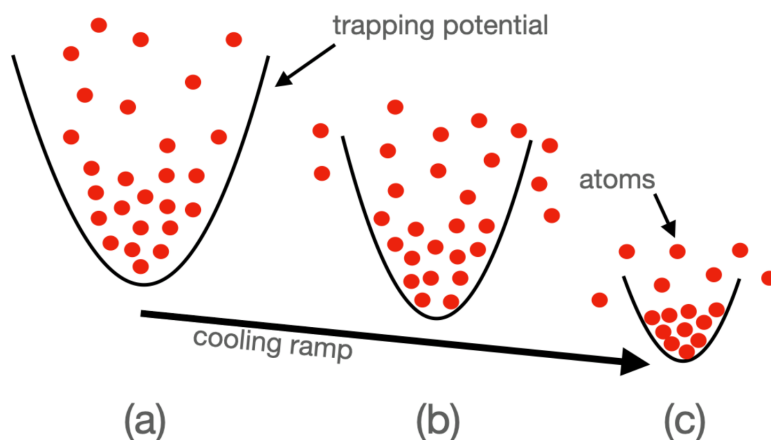


**Figure 2.4: Evaporative cooling process.** (a) Atoms are trapped in potential walls. (b) By lowering the potential walls, we enable high-energy atoms to escape. (c) rethermalization of the remaining atoms, decreasing the atomic cloud temperature. We repeat (b) and (c) until reaching the needed BEC tempearture.

The efficiency of this cooling technique is quantified by the increase of the phase space density (PSD). It is defined by

$$D = n\lambda_{dB}^3 \quad \text{with} \quad \lambda_{dB} = \sqrt{\frac{2\pi\hbar^2}{mk_B T}} \quad (2.11)$$

where  $\lambda_{dB}$  is the thermal de Broglie wavelength – used to describe the length scale of the individual atomic wavefunction – and  $n$  is the atomic density.

We consider here three-dimensional harmonic traps, so the PSD is given by

$$D = N \left( \frac{\hbar\bar{\omega}}{k_B T} \right)^3 \quad \text{with} \quad \bar{\omega} = (\omega_x\omega_y\omega_z)^{1/3}. \quad (2.12)$$

Our goal is to decrease both  $N$  and  $T$  in a way that increases the ratio  $N/T^3$ . One can show[15][16] that Bose-Einstein condensation occurs beyond the limit of  $\zeta(3) \approx 1.202$ . A Bose-Einstein condensate (BEC) is a phase of matter, typically bosonic particles, that mostly occupy the lowest-energy quantum state. In this state of matter, quantum phenomena become apparent macroscopically, enabling the study of rich physics. An example of PSD increase and thus BEC formation is given below in fig 2.5:

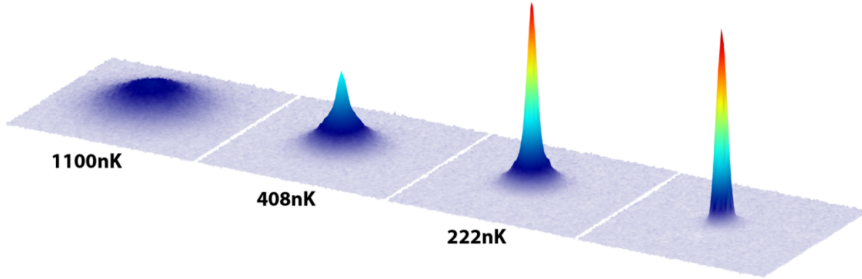


Figure 2.5: BEC formation using Erbium atoms.[17]

Since we “sacrifice” atoms during this process, it is mandatory to have a sufficient enough number of atoms transferred to the science cell to get a BEC, **which therefore motivates our technical upgrade**. Currently, the ongoing projects only require thermal clouds of about  $5 \times 10^4$  atoms at temperatures around  $0.2 \mu K$ , but being able to easily produce BECs would open the door to various exciting new projects.

## 2.4 Outlook

In this chapter, we saw that the number of atoms trapped in the science cell at the end of the apparatus is a key parameter to perform various physics experiments. Indeed, enough atoms enable for instance Bose-Einstein condensation. As we discussed, a non-negligible number of atoms are lost while transporting them from the MOT

to the science cell, especially during the loading phases. We will discuss in the next chapter a setup upgrade that addresses this issue.

# Chapter 3

## Improving the transport laser

As mentioned in the previous chapter, we need a better spatial overlap between traps in the loading steps of the atom transport. An efficient technique to do so is to artificially increase the width of a laser beam and thus tuning the aspect ratio of an ODT is by using spatial modulation. Such techniques have been used for instance to produce double well potentials[18].

In this chapter, we will first introduce the principle of atomic cloud shape tuning using acousto-optic modulation, we will then describe the experimental setup built to test it, before giving our results.

### 3.1 Theory and simulations

#### 3.1.1 Principle of time-averaged potentials

The principle is to move the position of the ODT periodically in order to create an averaged dipole trap which will have a different shape. Indeed, it can increase the trap width, while reducing the trap depth to keep the volume constant. Such technique, sometimes known as *painting*, is realized by spatially modulating the transport beam in the transverse direction.

The relevant trap frequency to consider is then  $\omega_\rho$ , and is our reference for the modulation frequency  $\omega$ . We can distinguish three situations:

- $\omega \ll \omega_\rho$  : the atoms will follow the trap adiabatically. Although it does not induce loss of atoms, this is of no interest.
- $\omega \approx \omega_\rho$  : this can induce resonant excitation of the center-of-mass motion mode of the atomic cloud. As it would lead to heating the atoms, this case is to be avoided.

- $\omega \gg \omega_\rho$  : the atomic cloud will only see a time-averaged intensity profile. This last situation is precisely the desired one[19].

Let  $\rho_0(t)$  be the modulation function of amplitude  $A$ . For instance, a sinusoidal modulation would be given by

$$\rho_0 = A \sin\left(2\pi \frac{t}{T}\right). \quad (3.1)$$

Over one period of oscillation  $T$  while the center of the trap  $\rho_0$  moves periodically, we can compute averaged trapping potential  $V$  as

$$V(\rho) = \frac{1}{T} \int_{-T/2}^{T/2} dt U(\rho - \rho_0(t)). \quad (3.2)$$

In this formula,  $U(\rho) = -U_0 \exp(-2\rho^2/w_0^2)$  is the trapping potential in the focal plane and in an arbitrary transverse direction  $\rho$ .

By restricting ourselves to modulation functions monotonically increasing over the first half-period and decreasing in the second one, we can restrict the integral over only the first half of the period. This enable us to perform a change of variable with  $\rho_0 = f(2\pi t/T)$ , leading to

$$\begin{aligned} V(\rho) &= \frac{1}{T} \int_{-T/2}^{T/2} dt U(\rho - \rho_0(t)) \\ &= \frac{2}{T} \int_{-T/4}^{T/4} dt U(\rho - \rho_0(t)) \\ &= \int_{-A}^A d\rho_0 \Pi(\rho_0) U(\rho - \rho_0). \end{aligned} \quad (3.3)$$

We thus see that the averaged trap potential is the convolution product of the regular potential profile  $U(\rho)$  and a gate function  $\Pi(\rho)$  given by

$$\Pi(\rho) = \frac{1}{\pi} \frac{1}{(f' \circ f^{-1})(\rho)} \quad (3.4)$$

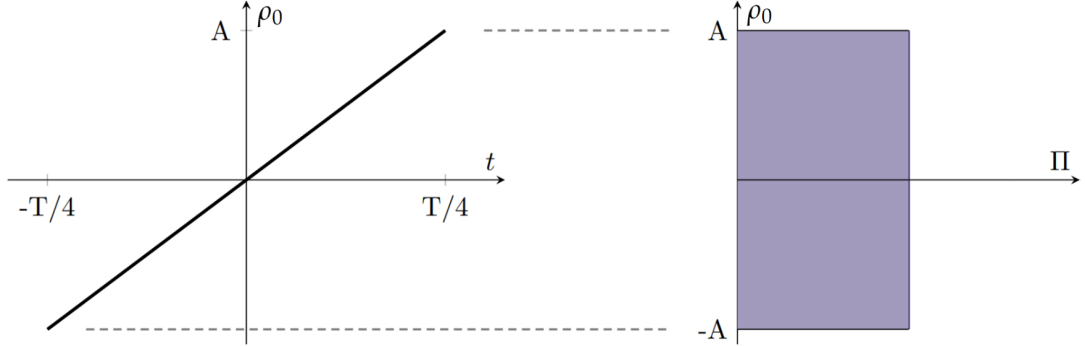
and normalized according to

$$\int_{-A}^A \Pi(\rho) d\rho = 1.$$

### 3.1.2 Choice of the modulation function

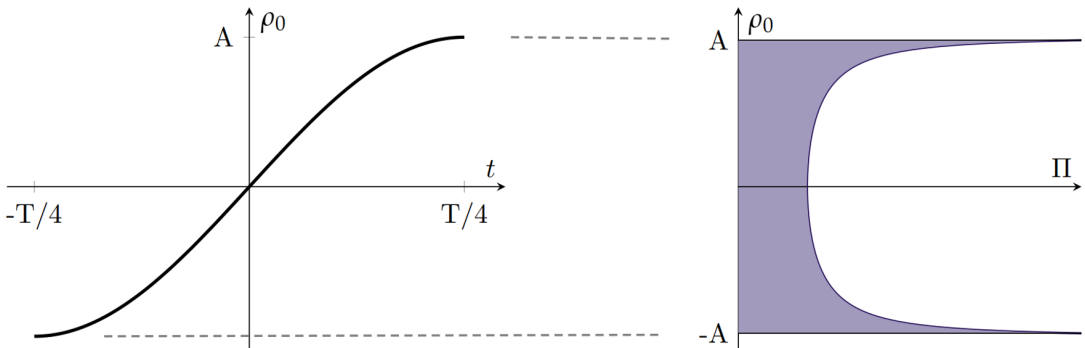
Following the work from [20], we can consider a few examples of modulation shapes and their associated gate function :

- **Linear modulation.** This leads to an uniform distribution, because the beam spends an equivalent time at each position.



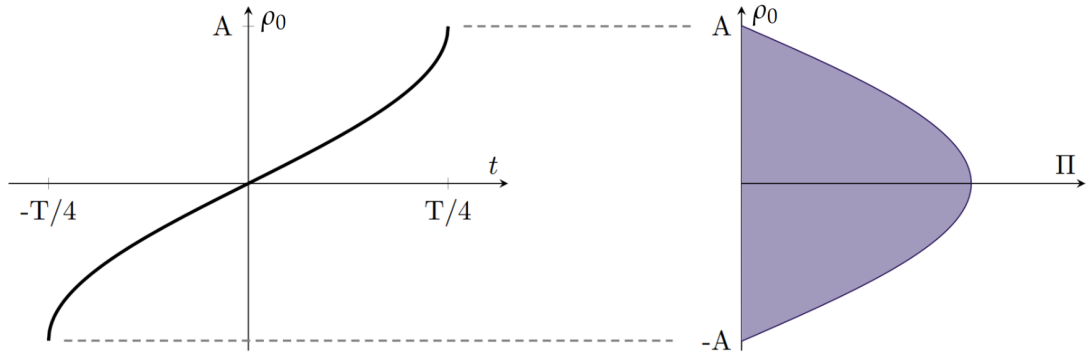
- **Sinus modulation.** Since the beam spends more time one the edges, it leads to divergences of the gate distribution. One can show that

$$\Pi(\rho) = \frac{1}{\pi A} \frac{1}{\sqrt{1 - \rho^2/A^2}}. \quad (3.5)$$



- **Arcsinus modulation.** We predict here the opposite behavior. One can show that  $\Pi$  is given by :

$$\Pi(\rho) = \frac{\pi}{4A} \cos\left(\frac{\pi\rho}{2A}\right). \quad (3.6)$$



To investigate which function would be the best for our work, we simulate the different trap potentials, both in one dimension - in the  $z = 0$  plane - and two dimensions. In the following figures,  $A$  and  $\rho$  are expressed in units of the beam waist  $w_0$ , and  $z$  expressed in units of  $z_R$ .

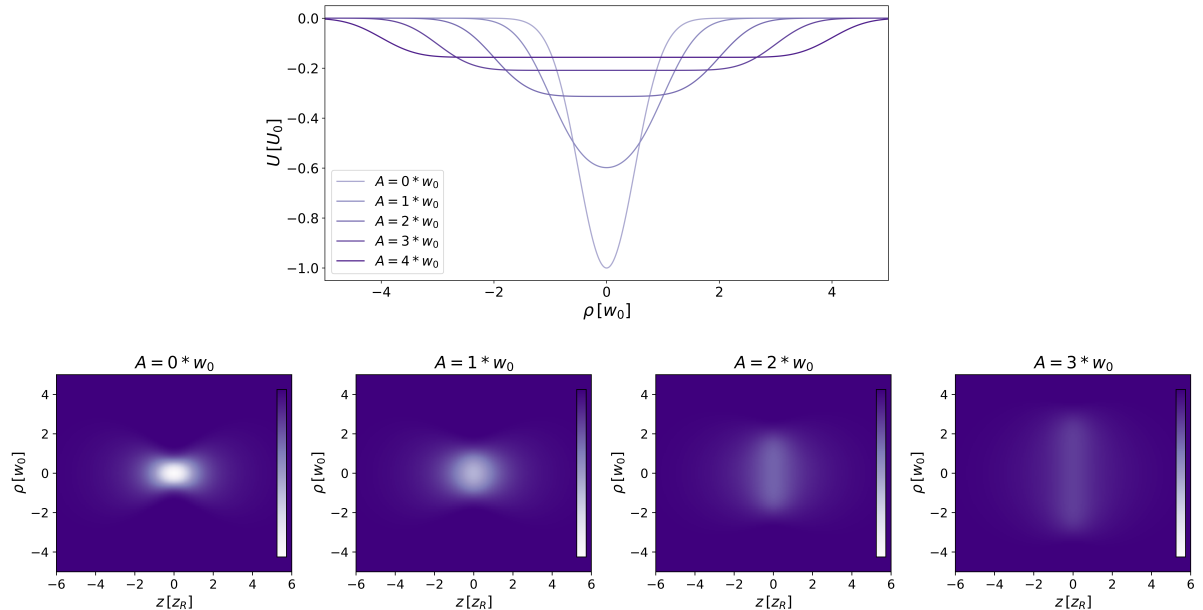


**Figure 3.1: Averaged trap for a linear modulation and different values of  $A$ .**  
We obtain a flat-bottom trap, which should be avoided.

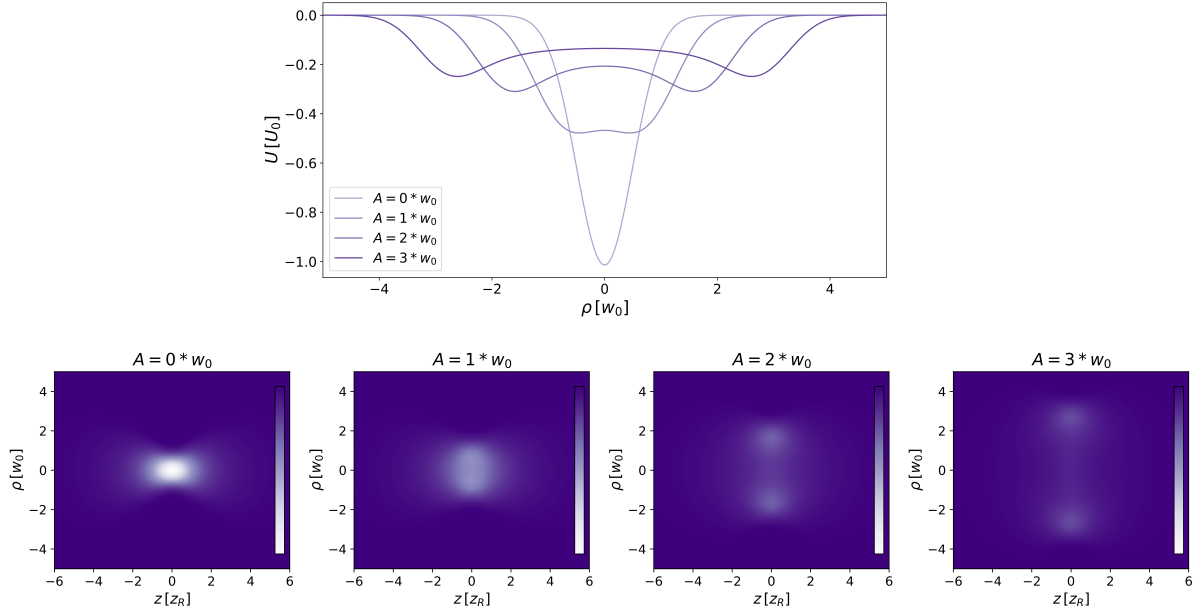


**Figure 3.2: Averaged trap for a sinus modulation and different values of  $A$ .**  
We observe the apparition of local minima, which is harmful to our atom trapping.

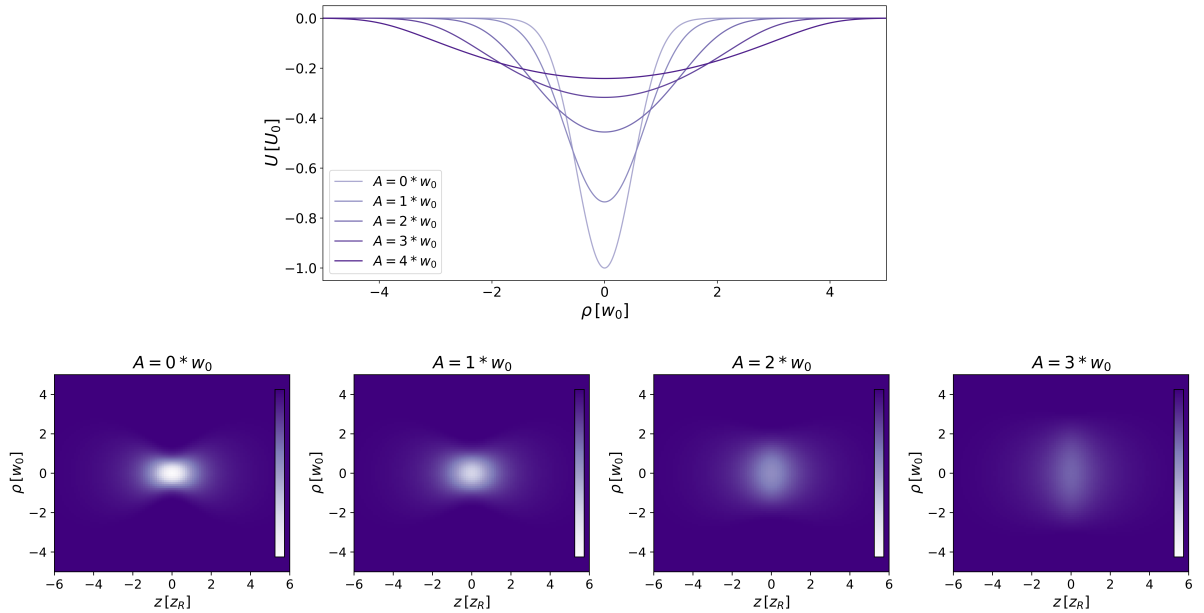


**Figure 3.3: Averaged trap for an arcsinus modulation and different values of  $A$ .**  
The trap is harmonic around its center, and similar to a Gaussian trap.

From those simulations, an **arcsinus function** seems to be the best modulation shape for our experiment. Indeed, it will allow us to use well-known results of cold atoms theory in harmonic traps.

### 3.1.3 Tuning the aspect ratio

In this section, we will focus on how the arcsinus modulation can be used to modify the aspect ratio of an atomic cloud. As we can see from equation (2.8), one can extract the trap frequencies from the potential, around its minimum. By fitting the previous simulations using a quadratic function around  $z = 0$ , we extract  $\omega_\rho$  and  $\omega_z$ . On the current transport laser setup, a 50 W IPG laser is used. To take in account some losses in the setup, we run our simulations for 45 W of optical power. We perform the fitting for various modulation amplitudes, and plot the frequencies behavior below:

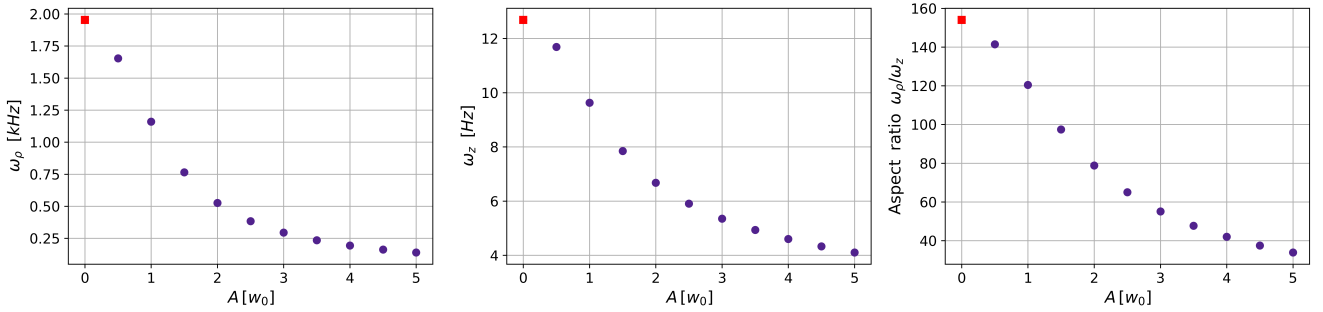


Figure 3.4: **Simulation of the trap frequencies with modulation.** From left to right, evolution the transverse and longitudinal frequencies, and aspect ratio. The red square corresponds to the current trap, without any modulation. 45 W of optical power are used.

As expected, the modulation decreases the transverse trap frequency, thus increasing the width of the average trap. Although the axial frequency decreases as well, the effect is weaker and we see that the aspect ratio improves. At first sight, the modulation technique seems to be efficient to enhance our transport setup. However, two points need to be considered:

- The trapping in the axial direction fixes the transport time, to make sure the transport is both adiabatic and fast enough to prevent from collisional atom losses. For these reasons, the current sequences used for the experiences should not be modified, therefore the technical upgrade should not modify the axial ODT frequency. As we can see from the middle plot above, the current axial frequency of the transport ODT is:

$$\omega_z = 12.68 \text{ Hz}$$

- Since the trap volume is kept constant, the modulation induces a decrease of the trap depth, that could lead to atom losses :

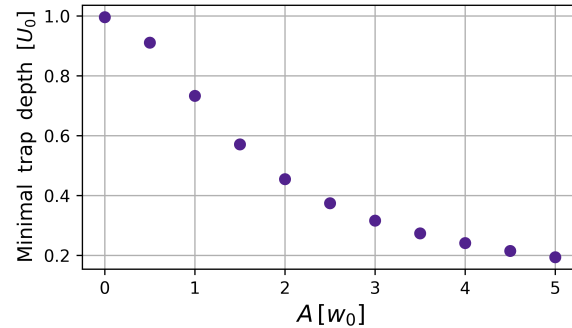


Figure 3.5: Trap depth is decreased by modulation.

A straightforward way to address these two issues is to increase the optical power on the atoms. The group had an available 300 W IPG laser that could be used for this purpose: we can then run again our simulations for an total power of 240 W on the atomic cloud, considering again some optical losses:

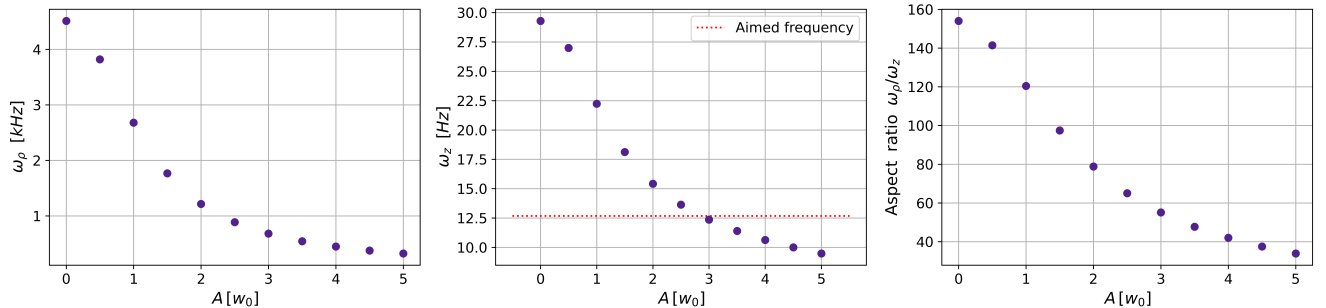


Figure 3.6: Similar simulations as in 3.4, but with 240 W of optical power.

From those results, we see that this increase of power would enable us to use the trap modulation with an amplitude up to  $A = 3 * w_0$  while keeping the axial frequency at its current value. In addition, we note that the evolution of the aspect ratio during modulation is independent of the power used, showing that the use of a more powerful laser will have no detrimental effect on the widening of the averaged trap.

One could also imagine that modulation would only be active during the loading phases of the atomic cloud (in the transport ODT and in the science cell cODT). In this

case, the transport time would remain unchanged, but the modulation would still result in a reduced trap depth. As the team has not yet decided which final case will be retained, we will focus our work on the first one, being the most restrictive.

Our simulations have therefore enabled us to guide the experimental implementation of this cloud shape tuning technique, using accousto-optic modulation of a laser beam.

**The two main points are as follows:**

- **modulation by an arcsine function is optimal,**
- **we need to increase laser power to implement this technique, so we'll be using the IPG 300 W laser.**

## 3.2 Experimental setup

### 3.2.1 New transport setup

Once that we had identified the main improvement directions of the setup, we had to build it in order to test these upgrades. A simplified scheme of the final test-setup is shown in figure 3.7. First, we used a 1% transmission mirror at the very beginning of the optical path, so we could work with only a few watts further in the setup, which is safer for both us and the equipments. The beam size is then reduced using a first telescope, which has been selected to optimize the AOM performances. Just before the AOM, we use a half-wave plate in order to tune the light polarization to an optimal direction. At the AOM output, we cut the non-diffracted order using a moon-shaped mirror in the focal plane of a  $f = 75\text{ mm}$  lens. Indeed, this lens is part of a second telescope needed to greatly increase the beam size. The first order, enlarged thanks to this configuration, is then passing through the focusing lens, leading to the desired beam waist in its focal plane where we place the camera, and where the atomic cloud will be in the real setup.

The electrical setup to monitor the RF signal sent to the AOM can be described as follows:

- A waveform generator sends a voltage to a Voltage Controlled Oscillator<sup>1</sup> (VCO) with the desired waveform, depending on the desired frequency.

---

<sup>1</sup>Mini-circuits ZOS-150+

- The VCO then sends a RF signal to a Voltage Variable Attenuator<sup>2</sup> (VVA) that enables us to monitor the RF power, and thus the fraction of the beam going into the non-diffracted or first order.
- The signal is amplified before reaching the AOM.

We will discuss in the next sections the difficulties encountered and the choices made when designing and building this setup.

---

<sup>2</sup>Mini-circuits ZX73-2500- S+

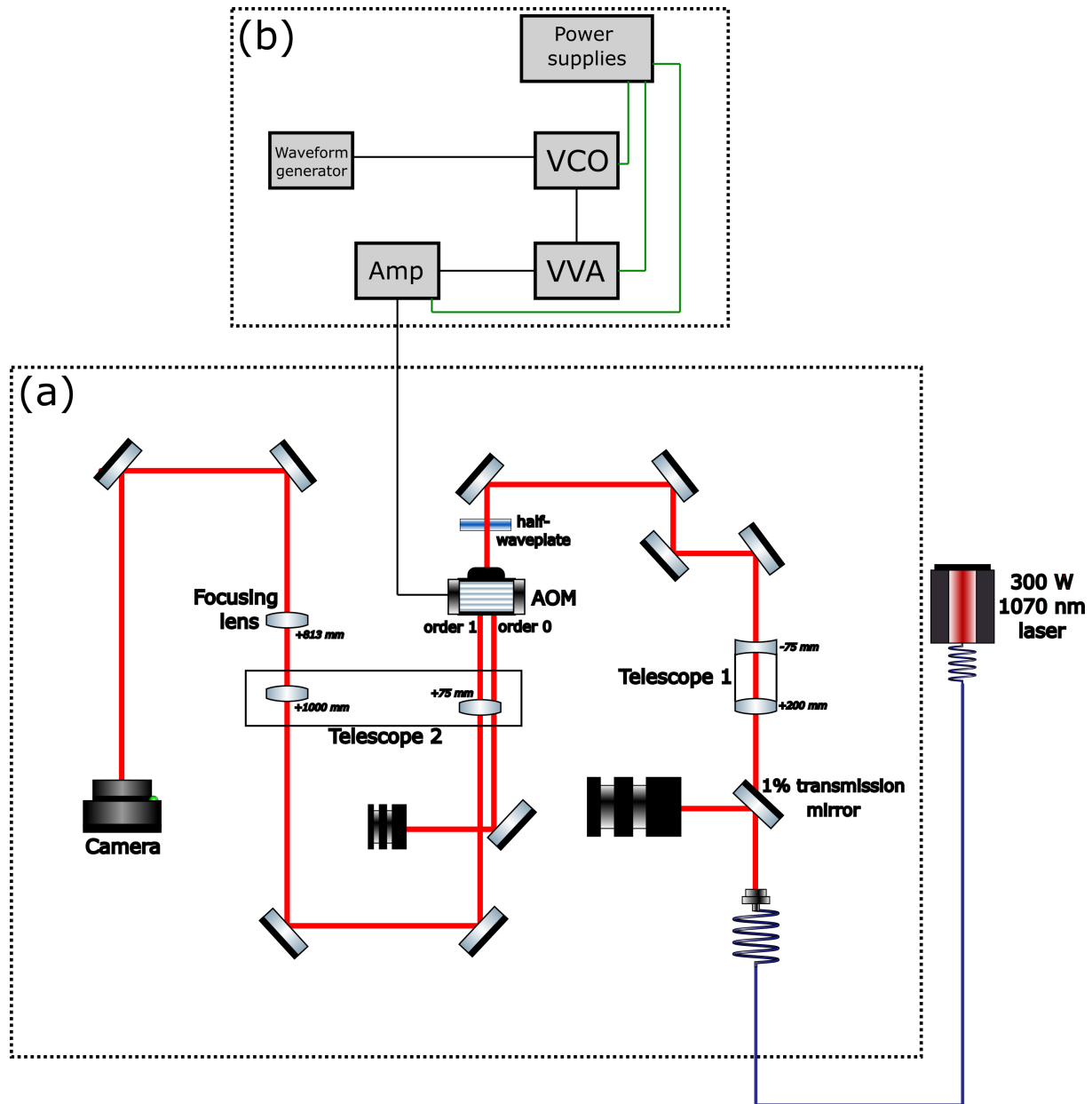


Figure 3.7: **Simplified scheme of the new transport setup.** (a) Optical part of the setup. Some minor components, for instance those used to handle light reflections, are not displayed. (b) Electrical connections of the AOM.

### 3.2.2 Imaging the beam

As we presented earlier, our goal is to induce periodic translation of the trap, thus the laser beam. Most of our data taken for this work are then images of the beam, using

a CMOS camera<sup>3</sup>, orthogonal to the propagation axis. The image is displayed with the software DataRay, and exported to Python for analysis.

To extract the main features of the beam, we fit the image by a two-dimensional elliptical Gaussian function, that reads

$$f(x, y) = A \exp \left[ -2 \left( a(x - x_0)^2 + b(x - x_0)(y - y_0) + c(y - y_0)^2 \right) \right] \quad (3.7)$$

where  $x$  and  $y$  are 2 orthogonal directions in the transverse plane corresponding to  $w_x$  and  $w_y$ , the two waists of the 2D gaussian tilted by an angle  $\theta$ , such as:

$$\begin{aligned} a &= \frac{\cos^2(\theta)}{w_x^2} + \frac{\sin^2(\theta)}{w_y^2} \\ b &= -\frac{\sin(2\theta)}{w_x^2} + \frac{\sin(2\theta)}{w_y^2} \\ c &= \frac{\sin^2(\theta)}{w_x^2} + \frac{\cos^2(\theta)}{w_y^2}. \end{aligned}$$

An example is given in fig 3.8 below:

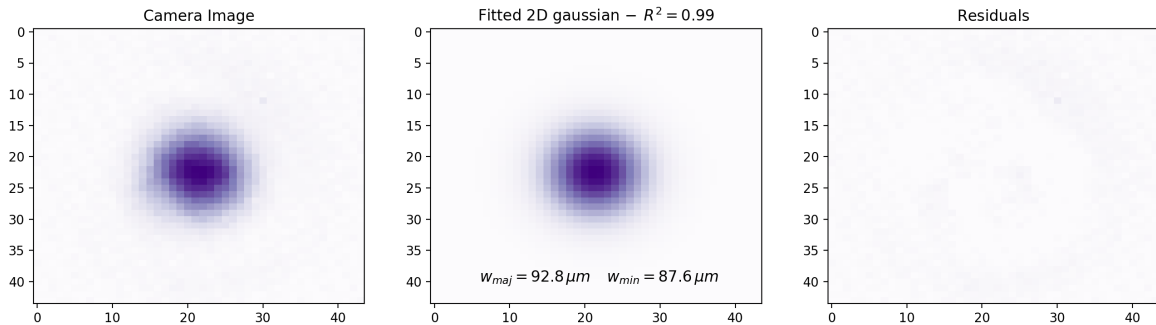


**Figure 3.8: Typical imaging of the beam.** The axis are given in pixel numbers, with one pixel being  $9.3 \times 9.3 \text{ mm}^2$  for our camera. We extract from the fit the major axis  $w_{maj}$  and the minor one  $w_{min}$ . The residuals are given by the difference between the fit and the original data.

By extracting the waists and the amplitude from the fit, we can study the performance of our new optical setup and guide further improvements, as discussed in the next parts.

---

<sup>3</sup>DataRay WinCamD

### 3.2.3 Working with high power

One of the main difficulties of this work was to work with such a high-power laser. Indeed, building an optical setup based on a 300 W laser beam involves a lot of preparatory work to ensure both safety of the experimenter - myself - and the other optical and electrical components.

Building this setup required a great deal of adaptability to cope with the various concerns involved in working at high power. Since I think this may be useful to anyone planning to do similar work, I'll detail in this sub-section the various important points to consider.

First of all, we can ask ourselves whether our work on acousto-optic modulation of the laser beam can be carried out by lowering the laser power directly, and not at 300 W. To do this, we characterize the laser by studying the impact of power on the beam propagation. Our study is presented in the graph below:

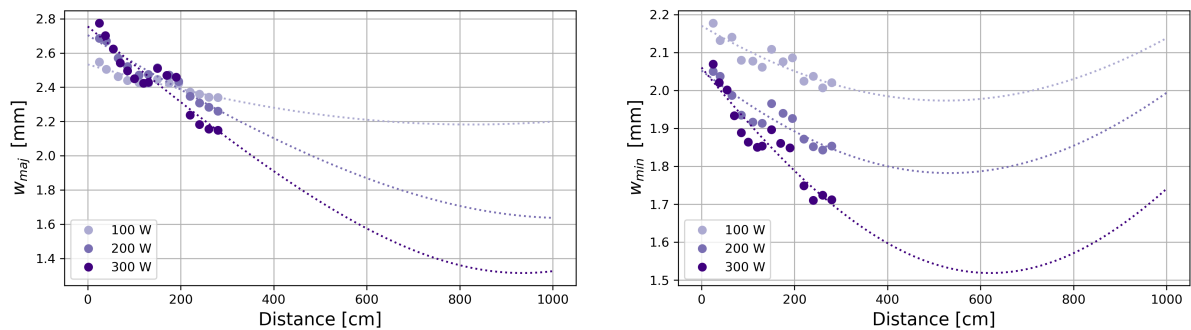


Figure 3.9: **Beam collimation for different output powers.** Major and minor waists are extracted from beam images at various distances, and the data are fitted using (2.3).

We clearly observe that the laser output power impacts the beam propagation. Therefore, our study has been pursued with a laser output power of 300 W, a fixed power identical to the experimental conditions.

However, we obviously cannot build a free-space optical setup with a 300 W beam, for various reasons:

- it is dangerous for the experimenter;
- classical Thorlabs mirror break when the beam is too small. We ordered high-power ones for Qioptic that should be resistant enough, but we only received them at the end of my stay, so they are still to be tested;
- the camera is not designed for high powers, and would melt instantly.

To reduce the optical power going through the setup, we first used a series of polarizing beam splitters (PBS) and half-wave plates to control the beam power by playing with its polarization. By rotating the waveplate, we can monitor which portion of the light will pass through the PBS, and which one will be reflected into a beam dump. Even if this works on paper, we observed that this technique could not be used in our case. The light going out of the laser is mostly coherent light with a well-defined polarization, but a small part is incoherent with random polarizations. Two {waveplate + PBS} systems in series were needed to decrease the power to a low enough value for imaging. However, the passage through each one increases greatly the ratio *incoherent/coherent* when minimizing the output power, leading at the end to a mostly incoherent mode, shown below:

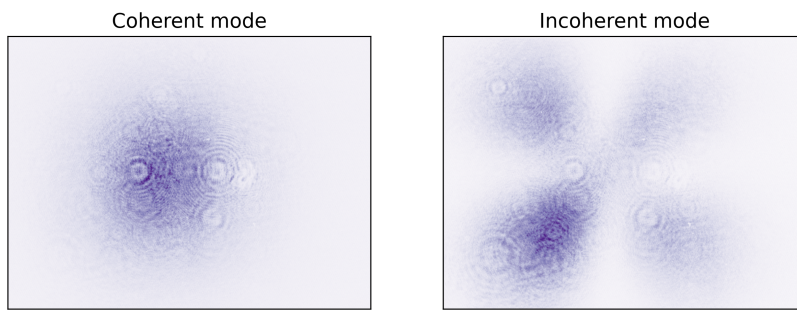


Figure 3.10: **Mode change with incoherent light.** One the left, with mostly coherent light, we have a Gaussian mode, close to the  $TE_{00}$  mode. On the right, with mostly incoherent light, one can recognize a  $TE_{11}$ -like mode.

Our first try to face this issue was to only use one {waveplate + PBS} system, along with a transmission mirror letting through a few percents of the light, the rest of it being reflected to a beam dump. Further investigations demonstrated that both the Thorlabs waveplates and high-power PBS were distorting the beam when directly exposed to 300 W, and we therefore decided to lower the optical power through the setup was the use of multiple transmission mirrors. Although this solution does not enable tuning the power, it prevents from critical optical aberrations and is thus the most suitable one.

Finally, it should be noted that the installation of a high-power experimental setup must be combined with a water-cooling system<sup>4</sup>, both for cooling the laser itself and the various beam dumps in the setup, that we built. It is worth noticing that this part of the building process requires neither advanced technical skills nor a great deal of thought, but is extremely time-consuming.

<sup>4</sup>using Lauda Microcool Circulation 1200 W chiller.

### 3.2.4 The acousto-optic modulator

The principle of an AOM is as follows: a collimated input beam passes through the AOM, which diffracts part of the light at an angle that depends on its working frequency. In our experiment, we use a modulator<sup>5</sup> with a central frequency  $\nu_0 = 80\text{ MHz}$ , whose 1st order is diffracted at an angle of around 15 mrad with respect to the non-diffracted 0 order. The working frequency of the AOM influences the first diffraction order, which is the one of interest in our work. The diffracted beam is then magnified by a telescope and focused on the atoms at a waist of around  $30\mu\text{m}$  to trap them (see fig 3.11). It can be shown that a frequency shift  $\delta\nu$  induces an angle  $\theta$  on the diffracted beam leaving the AOM, which in turn induces a shift in the position of the focal point in the focal plane of the last lens  $f_3$ . The relationship between those values is given by :

$$\delta = \frac{f_1 f_3}{f_2} \tan(\theta) \quad \text{with} \quad \theta = \frac{\lambda \delta\nu}{c} \quad (3.8)$$

with the focal lengths denoted in the figure 3.11,  $\lambda = 1070\text{ nm}$  and  $c = 5740\text{ m/s}$  is the sound speed in the AOM crystal quartz.

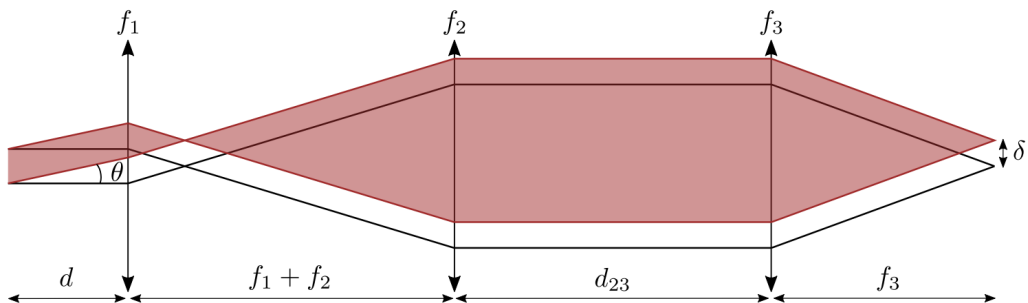


Figure 3.11: **Optical scheme of the beam modulation.** The black lines correspond to the first-order diffracted beam, for the AOM working at its central frequency  $\nu_0$ . The red lines denote the beam when tuning the AOM frequency to  $\nu_0 + \delta\nu$ , leading to a transverse position shift at the atoms.  $d$  relates to the distance between the AOM and the 3-lens optical system.

In practice, we choose an arbitrary value of  $d_{23}$ , small enough for space convenience. However, an important constraint exists on the distance that we introduced as  $d$ , between the AOM and the first lens. We indeed need that the AOM and the atoms are both in the focal planes of the optical system composed of the three lenses. It means that beams arriving to the telescope with slightly different angles – due to the modulation – will all focus in the same plane, i.e. their minimal waist positions will

---

<sup>5</sup>HG I-M080-2C10G-4-AM3

be aligned in the same plane (see fig 3.12). If this condition is not fulfilled, the shift of minimal waist plane during the modulation would induce a potential gradient attracting the atoms out of the trap, which should be strictly avoided. Using ray transfer matrix analysis, we can determine the optimal  $d$  value:

$$d = f_1 + \frac{f_1^2}{f_2} + \frac{f_1^2}{f_2^2}(f_3 - d_{23}) \quad (3.9)$$

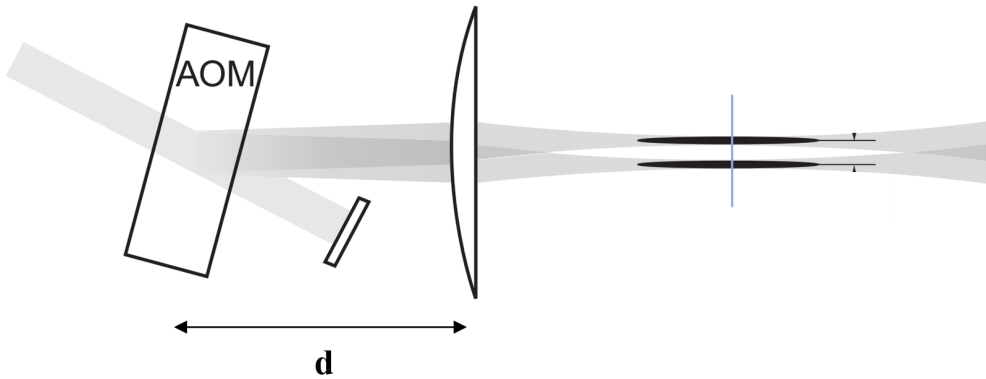


**Figure 3.12: Impact of the AOM position.** The distance  $d$  impacts the beam propagation in the optical system. For an optimal value, the position of minimal waists are in the same plane, for different beam angles at the AOM output. It is represented here by a blue transverse line. Adapted from [18].

In our setup, noting that  $d_{23}$  has here a negligible impact on this equation, we obtain  $d_{theo} = 85$  mm. By putting the two telescope lenses on translation stages, we characterize the impact of small variations of the distance  $d$  around its optimal calculated value, along with the impact of a huge variation. We obtain the following results:

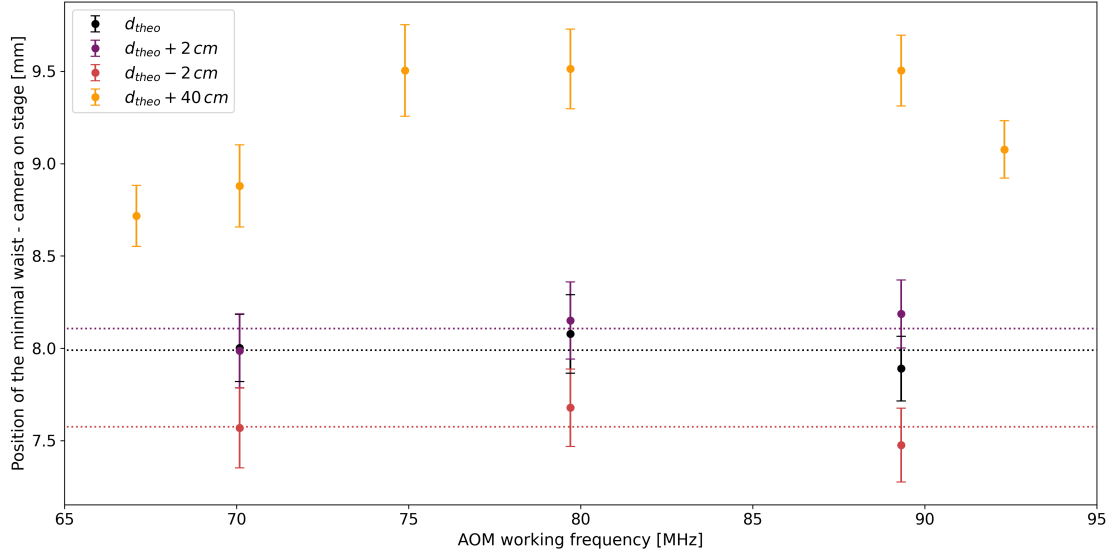


Figure 3.13: **Impact of the AOM position on the modulation.** As the dotted lines show, the modulation does not induce a change in the minimal waist position if the AOM is kept around  $d_{theo}$ . However, we observe that a bigger variation leads to these variations, making modulation impossible.

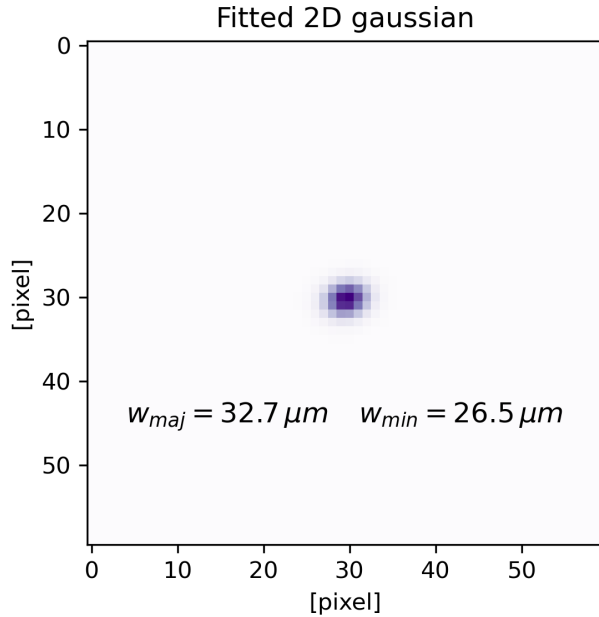
Our measurements confirm the importance of the AOM position for our project, while indicating that centimeter precision is not required.

In addition to this, we investigated the impact of the AOM input beam size on its efficiency. We observed that the effective diffraction zone on the crystal is smaller than the active aperture given in the documentation. Indeed, after testing different telescope configurations to send a narrowed beam into the AOM, we noticed that a slightly too large beam led to the observation of lateral fringes corresponding to the non-diffracted portion of the beam. Our study concluded that a  $\{+200\text{mm} / -75\text{mm}\}$  telescope, leading to a diffraction efficiency of 86% and an unclipped beam shape, offered optimal conditions for our work.

### 3.3 Modulation results

#### 3.3.1 Atom trapping configuration

The first requirement of our setup is to obtain a beam with a waist of around  $30 \mu\text{m}$  where the atoms will be, corresponding to the atomic cloud typical size on the current setup. This condition has been achieved, as shown in the following figure:



The slight ellipticity is typical of an experimental optical setup, being caused by non-perfect alignment and aberrations introduced by the optical elements used. This is not a problem for our work.

#### 3.3.2 Beam modulation

We then look at the evolution of the beam position during a discrete, slow variation in the VCO control voltage, and thus in the working frequency of the AOM. The linear evolution is described below:

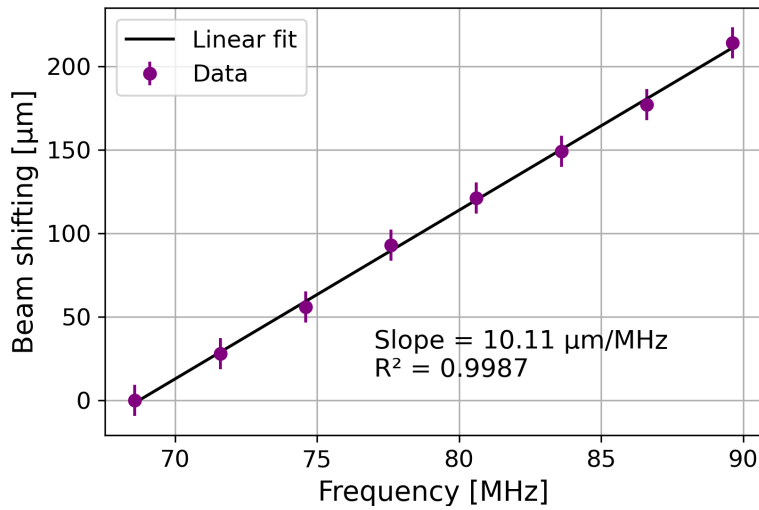
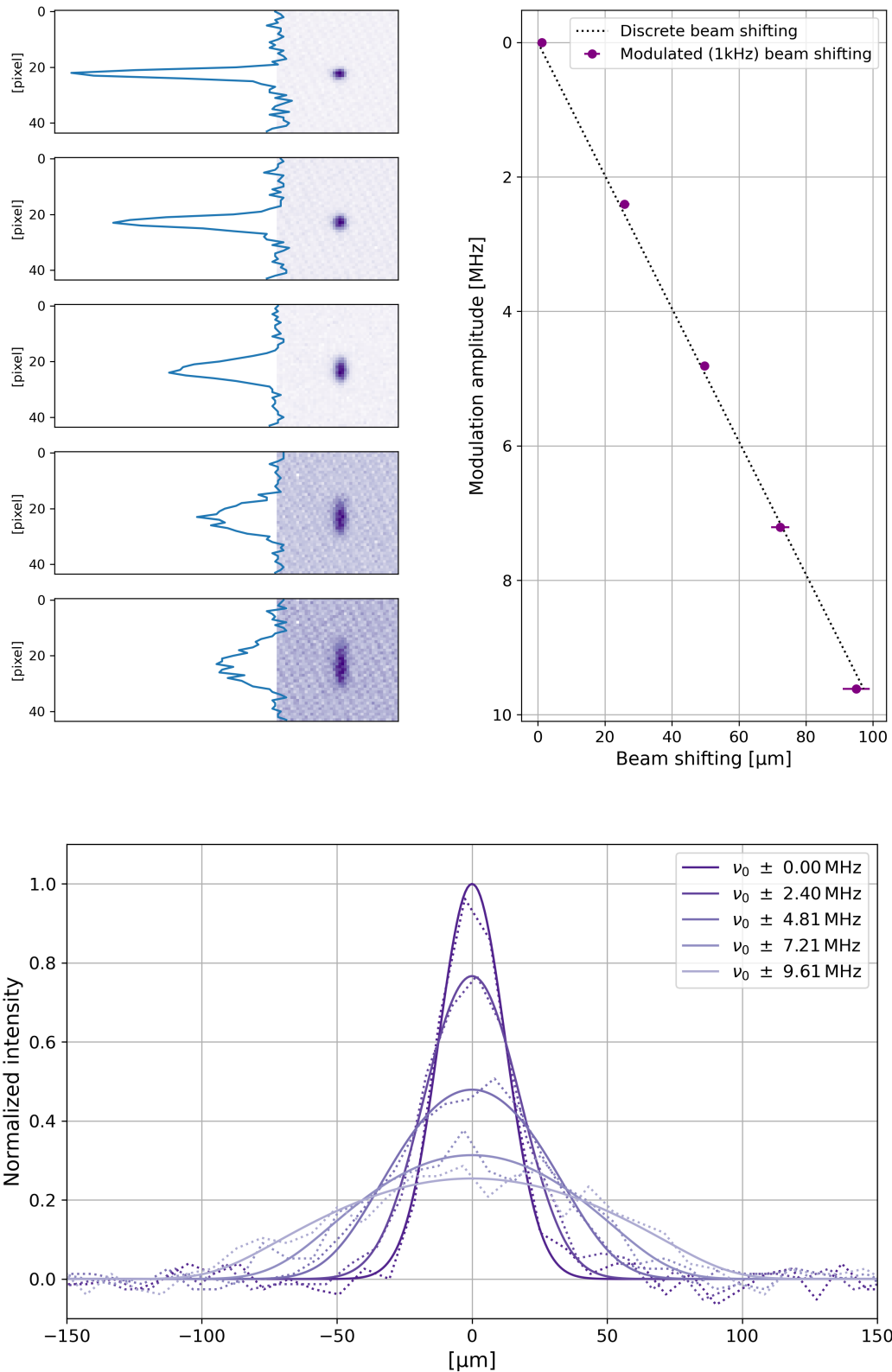


Figure 3.14: **Beam shifting for discrete variations of the AOM working frequency.**

Next, we can move on to the main objective of our study: testing beam modulation. To that end, we use a RIGOL waveform generator to vary the VCO control voltage. As determined earlier by our numerical simulations, we use an arcsine modulation, with a peak-to-peak amplitude of around 20 MHz around  $\nu_0$  and with a frequency  $\omega = 1\text{kHz}$  to start with. The modulation results are given below, from which we can extract the effective beam shifting by fitting the intensity profiles obtained in figure 3.15:



**Figure 3.15: Results for a 1 kHz arcsine modulation.** The upper plots show the averaged beam intensity when modulating and the associated beam shifts. The lower plot shows how these shifts are extracted.

We can see that modulation at 1kHz follows the expected behavior perfectly: the beam moves in accordance with the modulation amplitude applied. However, as shown in figure 3.7, the transverse trap frequency  $\omega_p$  is in the kilohertz range, so we need to modulate at a much higher frequency (see the subsection 3.1.1). By repeating the previous study with 100kHz modulation, we can see in figure 3.16 that the beam displacement is weaker than expected:

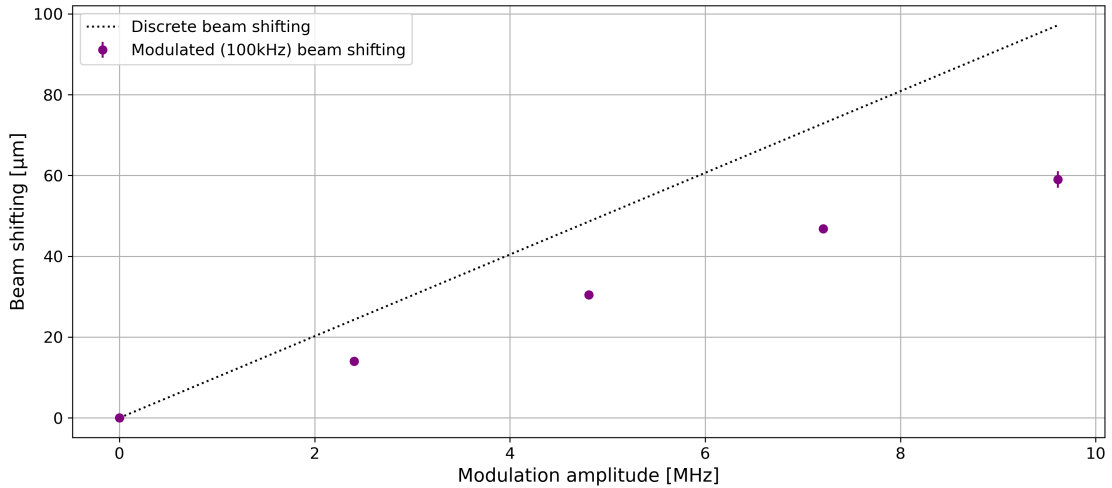


Figure 3.16: **Beam shifting for a 100 kHz modulation of the AOM working frequency.**

After several tests, we realized that this phenomenon originated not from the AOM, but from the VCO. In fact, the impedance of the VCO's drive source is resistive, whereas the VCO's tuning port is mainly capacitive. The VCO then acts as a first-order low-pass filter, which we characterized by measuring the beam displacement for different modulation frequencies. The results, fitted using a typical low-pass function, are given below in figure 3.17:

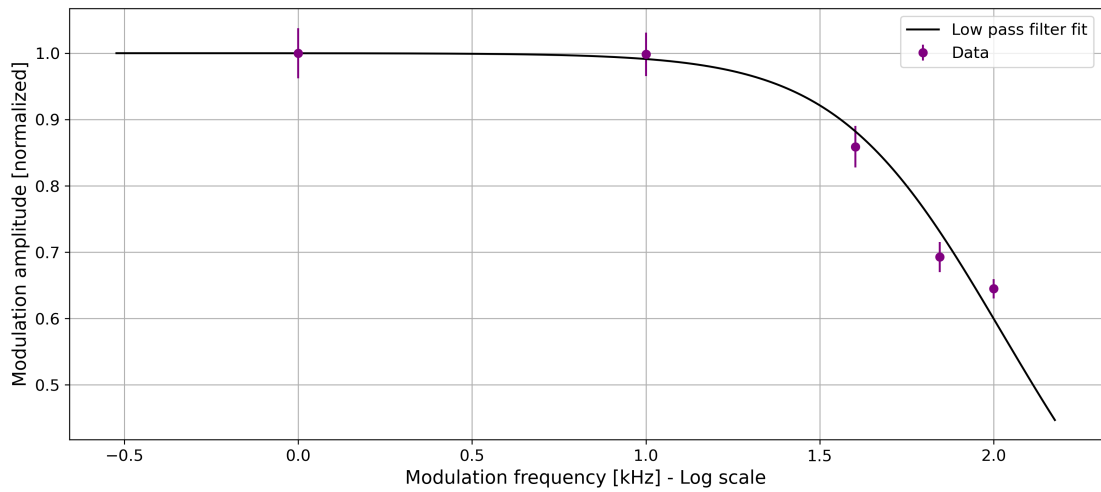


Figure 3.17: **First-order low-pass filter behavior of the VCO.** We notice a drop of the frequency delivered by the VCO when modulating its input voltage faster than 10 kHz.

To correctly modulate the AOM's working frequency at 100 kHz, one will just need to take this VCO limit into account, adapting the input voltage to compensate for the losses.

# Conclusion

To conclude this report, we have developed a new setup for the transport laser, using acousto-optic modulation and a high-power laser to improve the spatial overlap between traps in the loading steps of the atom transport. Now that this setup has been designed and tested, the next step would be to install it on the main apparatus and perform real atomic cloud shape tuning.

This upgrade will improve the number of atoms reaching the science cell, potentially leading to a new range of possible experiments, using for instance Bose-Einstein condensates.

# References

- [1] Richard P. Feynman. "Simulating physics with computers". In: *International Journal of Theoretical Physics* 21.6 (June 1982), pp. 467–488. ISSN: 1572-9575. DOI: [10.1007/BF02650179](https://doi.org/10.1007/BF02650179). URL: <https://doi.org/10.1007/BF02650179>.
- [2] Pascal Scholl et al. "Quantum simulation of 2D antiferromagnets with hundreds of Rydberg atoms". In: *Nature* 595.7866 (July 2021), pp. 233–238. ISSN: 1476-4687. DOI: [10.1038/s41586-021-03585-1](https://doi.org/10.1038/s41586-021-03585-1). URL: <https://doi.org/10.1038/s41586-021-03585-1>.
- [3] Immanuel Bloch, Jean Dalibard, and Wilhelm Zwerger. "Many-body physics with ultracold gases". In: *Rev. Mod. Phys.* 80 (3 July 2008), pp. 885–964. DOI: [10.1103/RevModPhys.80.885](https://doi.org/10.1103/RevModPhys.80.885). URL: <https://link.aps.org/doi/10.1103/RevModPhys.80.885>.
- [4] Immanuel Bloch, Jean Dalibard, and Sylvain Nascimbène. "Quantum simulations with ultracold quantum gases". In: *Nature Physics* 8.4 (Apr. 2012), pp. 267–276. ISSN: 1745-2481. DOI: [10.1038/nphys2259](https://doi.org/10.1038/nphys2259). URL: <https://doi.org/10.1038/nphys2259>.
- [5] Y.-J. Lin et al. "Synthetic magnetic fields for ultracold neutral atoms". In: *Nature* 462.7273 (Dec. 2009), pp. 628–632. ISSN: 1476-4687. DOI: [10.1038/nature08609](https://doi.org/10.1038/nature08609). URL: <https://doi.org/10.1038/nature08609>.
- [6] Thomas Chalopin et al. "Probing chiral edge dynamics and bulk topology of a synthetic Hall system". In: *Nature Physics* 16.10 (Oct. 2020), pp. 1017–1021. ISSN: 1745-2481. DOI: [10.1038/s41567-020-0942-5](https://doi.org/10.1038/s41567-020-0942-5). URL: <https://doi.org/10.1038/s41567-020-0942-5>.
- [7] Quentin Redon et al. *Realizing the entanglement Hamiltonian of a topological quantum Hall system*. 2023. arXiv: [2307.06251 \[cond-mat.quant-gas\]](https://arxiv.org/abs/2307.06251).
- [8] D. Dreon. "Designing and building an ultracold Dysprosium experiment : a new framework for light-spin interaction". PhD thesis. Université Paris Sciences Lettres, 2017.

- [9] C. Bouazza. "Ultracold dysprosium gas in optical dipole traps : control of interactions between highly magnetic atoms". PhD thesis. Université Paris Sciences Lettres, 2018.
- [10] T. Chalopin. "Quantum-enhanced sensing and synthetic Landau levels with ultracold dysprosium atoms". PhD thesis. Sorbonne université, 2019.
- [11] A. Fabre. "Realisation of Laughlin's topological charge pump in an atomic Hall cylinder". PhD thesis. Université Paris Sciences Lettres, 2022.
- [12] D. et al Dreon. "Optical cooling and trapping of highly magnetic atoms: the benefits of a spontaneous spin polarization". In: *Journal of Physics B: Atomic, Molecular and Optical Physics* 50.6 (Mar. 2017). DOI: [10.1088/1361-6455/aa5db5](https://doi.org/10.1088/1361-6455/aa5db5). URL: <https://iopscience.iop.org/article/10.1088/1361-6455/aa5db5>.
- [13] H. et al Li. "Optical trapping of ultracold dysprosium atoms: transition probabilities, dynamic dipole polarizabilities and van der Waals C<sub>6</sub> coefficients". In: *Journal of Physics B: Atomic, Molecular and Optical Physics* 50.1 (2017). DOI: [10.1088/1361-6455/50/1/014005](https://doi.org/10.1088/1361-6455/50/1/014005). URL: <https://iopscience.iop.org/article/10.1088/1361-6455/50/1/014005>.
- [14] Wolfgang Ketterle and N.J. Van Druten. "Evaporative Cooling of Trapped Atoms". In: ed. by Benjamin Bederson and Herbert Walther. Vol. 37. *Advances In Atomic, Molecular, and Optical Physics*. Academic Press, 1996, pp. 181–236. DOI: [https://doi.org/10.1016/S1049-250X\(08\)60101-9](https://doi.org/10.1016/S1049-250X(08)60101-9). URL: <https://www.sciencedirect.com/science/article/pii/S1049250X08601019>.
- [15] L. Pitaevskii and S. Stringari. *Bose-einstein condensation and superfluidity*. Oxford University PressOxford, 2016.
- [16] Franco Dalfovo et al. "Theory of Bose-Einstein condensation in trapped gases". In: *Rev. Mod. Phys.* 71 (3 Apr. 1999), pp. 463–512. DOI: [10.1103/RevModPhys.71.463](https://doi.org/10.1103/RevModPhys.71.463). URL: <https://link.aps.org/doi/10.1103/RevModPhys.71.463>.
- [17] K. Aikawa et al. "Bose-Einstein Condensation of Erbium". In: *Phys. Rev. Lett.* 108 (21 May 2012), p. 210401. DOI: [10.1103/PhysRevLett.108.210401](https://doi.org/10.1103/PhysRevLett.108.210401). URL: <https://link.aps.org/doi/10.1103/PhysRevLett.108.210401>.
- [18] Y. Shin et al. "Atom Interferometry with Bose-Einstein Condensates in a Double-Well Potential". In: *Phys. Rev. Lett.* 92 (5 Feb. 2004), p. 050405. DOI: [10.1103/PhysRevLett.92.050405](https://doi.org/10.1103/PhysRevLett.92.050405). URL: <https://link.aps.org/doi/10.1103/PhysRevLett.92.050405>.
- [19] R. Onofrio et al. "Surface Excitations of a Bose-Einstein Condensate". In: *Phys. Rev. Lett.* 84 (5 Jan. 2000), pp. 810–813. DOI: [10.1103/PhysRevLett.84.810](https://doi.org/10.1103/PhysRevLett.84.810). URL: <https://link.aps.org/doi/10.1103/PhysRevLett.84.810>.

- [20] A. Evrard. “Non-gaussian spin states of ultracold dysprosium atoms”. PhD thesis. Université Paris Sciences Lettres, 2020.